ANTIOXIDANTS & REDOX SIGNALING
Volume 20, Number 2, 2014

DOI: 10.1089/ars.2012.4616

Therapeutics

FORUM ORIGINAL RESEARCH COMMUNICATION

Monoamine Oxidase B Prompts Mitochondrial and Cardiac Dysfunction in Pressure Overloaded Hearts

Nina Kaludercic,[1] Andrea Carpi,[2] Takahiro Nagayama,[3] Vidhya Sivakumaran,[3] Guangshuo Zhu,[3] Edwin W. Lai,[4] Djahida Bedja,[5] Agnese De Mario,[6] Kevin Chen,[7] Kathleen L. Gabrielson,[5] Merry L. Lindsey,[8] Karel Pacak,[4] Eiki Takimoto,[3] Jean C. Shih,[7,9] David A. Kass,[3] Fabio Di Lisa,[1,6] and Nazareno Paolocci[3,10]

Abstract

Aims: Monoamine oxidases (MAOs) are mitochondrial flavoenzymes responsible for neurotransmitter and biogenic amines catabolism. MAO-A contributes to heart failure progression *via* enhanced norepinephrine catabolism and oxidative stress. The potential pathogenetic role of the isoenzyme MAO-B in cardiac diseases is currently unknown. Moreover, it is has not been determined yet whether MAO activation can directly affect mitochondrial function. ***Results:*** In wild type mice, pressure overload induced by transverse aortic constriction (TAC) resulted in enhanced dopamine catabolism, left ventricular (LV) remodeling, and dysfunction. Conversely, mice lacking MAO-B (MAO-$B^{-/-}$) subjected to TAC maintained concentric hypertrophy accompanied by extracellular signal regulated kinase (ERK)1/2 activation, and preserved LV function, both at early (3 weeks) and late stages (9 weeks). Enhanced MAO activation triggered oxidative stress, and dropped mitochondrial membrane potential in the presence of ATP synthase inhibitor oligomycin both in neonatal and adult cardiomyocytes. The MAO-B inhibitor pargyline completely offset this change, suggesting that MAO activation induces a latent mitochondrial dysfunction, causing these organelles to hydrolyze ATP. Moreover, MAO-dependent aldehyde formation due to inhibition of aldehyde dehydrogenase 2 activity also contributed to alter mitochondrial bioenergetics. ***Innovation:*** Our study unravels a novel role for MAO-B in the pathogenesis of heart failure, showing that both MAO-driven reactive oxygen species production and impaired aldehyde metabolism affect mitochondrial function. ***Conclusion:*** Under conditions of chronic hemodynamic stress, enhanced MAO-B activity is a major determinant of cardiac structural and functional disarrangement. Both increased oxidative stress and the accumulation of aldehyde intermediates are likely liable for these adverse morphological and mechanical changes by directly targeting mitochondria. *Antioxid. Redox Signal.* 20, 267–280.

Introduction

Monoamine oxidases (MAOs) are flavoenzymes located within the outer mitochondrial membrane. They are responsible for the oxidative deamination of neurotransmitters and dietary amines. In central neurotransmission, MAO activity terminates the action of catecholamines, such as norepinephrine, dopamine, and other neurotransmitters, such as serotonin. MAO inhibition has proven beneficial in mood disorders or Parkinson's disease (7, 43). In stark contrast, the impact of MAO activation on cardiac structure and function remains a relatively uncharted territory, particularly under stress conditions.

[1]Neuroscience Institute, National Research Council of Italy, Padova, Italy.
[2]Department of Experimental Oncology, European Institute of Oncology, Milano, Italy.
[3]Division of Cardiology, Johns Hopkins Medical Institutions, Baltimore, Maryland.
[4]Section on Medical Neuroendocrinology, NICHD, NIH, Bethesda, Maryland.
[5]Department of Comparative Pathobiology, Johns Hopkins Medical Institutions, Baltimore, Maryland.
[6]Department of Biomedical Sciences, University of Padova, Padova, Italy.
[7]Department of Pharmacology and Pharmaceutical Sciences, University of Southern California, Los Angeles, California.
[8]Division of Geriatrics, Gerontology and Palliative Medicine, San Antonio Cardiovascular Proteomics Center, The University of Texas Health Science Center, San Antonio, Texas.
[9]Department of Cell and Neurobiology, Keck School of Medicine, University of Southern California, Los Angeles, California.
[10]Department of Clinical and Experimental Medicine, University of Perugia, Perugia, Italy.

Innovation

Monoamine oxidase (MAO)-B isoform is highly abundant in the human heart, but its role and contribution to the maintenance of cardiac geometry and function have never been disclosed before. We show that presence of MAO-B is required for proper catecholamine clearance and cardiac function. Under stress conditions, such as pressure overload, MAO-B activity contributes to oxidative stress, structural, and functional derangements of the heart. Furthermore, we show that there is a direct relationship between products of MAO activity, oxidative stress and mitochondrial dysfunction. Present findings contribute to better understanding of cardiac diseases and pave the way to *ad hoc* designed therapeutic strategies.

The cardiac muscle is constantly exposed to the modulatory influence of neurohormones, either released by the sympathetic efferent fibers, that is, norepinephrine and dopamine, or by the adrenal gland, that is, epinephrine. Many chronic diseases, eventually culminating in heart failure, are characterized by an augmented entry of catecholamines into the myocardium, *via* upregulated extraneuronal monoamine transporter activity (16, 17). This event, in turn, enhances the catabolic capacity of MAO isoenzymes. Consistent with this scenario, our recent findings demonstrate that pharmacological or genetic inhibition of MAO-A prevents the occurrence of heart failure in pressure-overloaded mice (25). This salutary action stems from both the prevention of H_2O_2-driven oxidative stress/tissue apoptosis in the cardiac muscle, and the improved bio-availability of intra-neuronal norepinephrine. The latter phenomenon is due to its preserved neuronal re-uptake, *via* maintained function of the neuronal norepinephrine transporter. Together, these events concur to maintain proper left ventricular (LV) morphology and function, even under conditions of chronic cardiac stress due to pressure overload (3, 4, 39). As a major source of reactive oxygen species (ROS), MAO-A contributes to *in vitro* myocyte hypertrophy (6), ischemia/reperfusion (I/R) injury both in *ex vivo* (10) and *in vivo* models (5, 31), heart failure and LV remodeling (25, 42).

Until now, the attention has been focused on MAO-A, since it is the predominant isoform expressed in rat heart (15, 27, 36). However, MAO-B is highly abundant in the myocardium of species, such as mice and humans (15, 36). Notwithstanding, virtually nothing is known about its possible influence on myocardial structure and function.

On the basis of their substrate specificity and inhibitor sensitivity (43), MAOs are differentiated in isoform A and B. However, both of them catalyze the same oxidative deamination reaction that results in the formation of the corresponding aldehyde intermediate, ammonia and H_2O_2. The aldehyde intermediate is rapidly metabolized to corresponding acid by the action of aldehyde dehydrogenase (ALDH). More specifically, MAO-B converts the substrate dopamine, to 3,4-dehydroxyphenylacetaldehyde (DOPAL) (7), a very reactive aldehyde intermediate (Fig. 1A). DOPAL is then readily transformed in 3,4-dehydroxyphenylacetic acid (DOPAC) due to the action of ALDH. In turn, DOPAC is further converted by catechol-O-methyl transferase to the final product, homovanillic acid. Thus, the complete catabolism of monoamines, operated by both isoforms, produces not only H_2O_2 but also aldehydes and ammonia. This aspect is often overlooked when the consequences of MAO activation are being evaluated, either *in vitro* or *in vivo*. Yet, deficient ALDH activity may lead to the accumulation of aldehyde intermediates that are toxic, and likely exacerbating H_2O_2-driven oxidative stress. Consistent with this view is the fact that stimulating ALDH2 activity, the most abundant cardiac ALDH isoform localized within the mitochondrial matrix, grants protection against I/R mediated cardiac injury (11) and diabetic cardiomyopathy (44). Furthermore, these aldehydes are very reactive molecules that may lead also to mitochondrial dysfunction and eventually cell death (9, 34).

In the present study, we first tested whether MAO-B activity is centrally involved in the transition from compensated (concentric) hypertrophy to adverse LV remodeling and pump failure in pressure overloaded hearts. Second, we aimed to establish whether enhanced MAO activity *per se* can be a major cause of mitochondrial dysfunction.

Results

MAO-B$^{-/-}$ mice show compensated hypertrophy after 3 and 9 weeks of pressure overload

Whether MAO-B activity is involved in the transition from compensated hypertrophy to overt heart failure in pressure-overloaded hearts is unknown. To address this deficiency, we used MAO-B$^{-/-}$ mice and their 129/Sv wild type (WT) littermates. MAO-B$^{-/-}$ mice completely lack MAO-B activity in the heart (Supplementary Fig. S1A; Supplementary Data are available online at www.liebertpub.com/ars), whereas MAO-A gene expression and activity are intact (Supplementary Fig. S1B, C). Since the cardiac phenotype of MAO-B$^{-/-}$ mice has never been characterized before, we first performed echocardiographic measurements at baseline. As shown in Figure 1, there was no apparent difference between null and WT mice, either in terms of LV chamber dimensions, wall thickness or function.

Next, we subjected WT and MAO-B$^{-/-}$ mice to transverse aortic constriction (TAC), performing serial echocardiographic evaluation at 3 and 9 weeks after TAC. After 3 weeks, interventricular septum (IVS) and left ventricular posterior wall (LVPW) were increased in MAO-B$^{-/-}$ mice, along with LV mass that was higher in MAO-B$^{-/-}$ mice when compared to their WT littermates (Fig. 1). Together, these data indicate that, when subjected to pressure overload, MAO-B$^{-/-}$ mice developed more hypertrophy. However, in stark contrast to WT, MAO-B$^{-/-}$ mice displayed compensated LV function. Typically, 9 weeks after TAC hearts undergo overt LV remodeling and exhibit pump dysfunction (25, 37), as was the case with WT mice. In these mice, TAC produced an enlargement of LV end-systolic and end-diastolic diameters, consistent with the occurrence of LV dilation at this stage in other mouse strains (37). In stark contrast, adverse LV chamber remodeling was not present in MAO-B$^{-/-}$ mice whose LV dimensions remained comparable to those found in sham-operated animals (Fig. 1). Moreover, LV pump function, indexed by fractional shortening (FS), was markedly reduced in WT mice, but not in MAO-B$^{-/-}$ mice (Fig. 1). Since WT littermates and MAO-B$^{-/-}$ mice displayed similar levels of hypertrophy (IVS, LVPW and LVmass/body weight, Fig. 1), this set of data suggests that MAO-B$^{-/-}$ maintained a status of concentric, compensated hypertrophy.

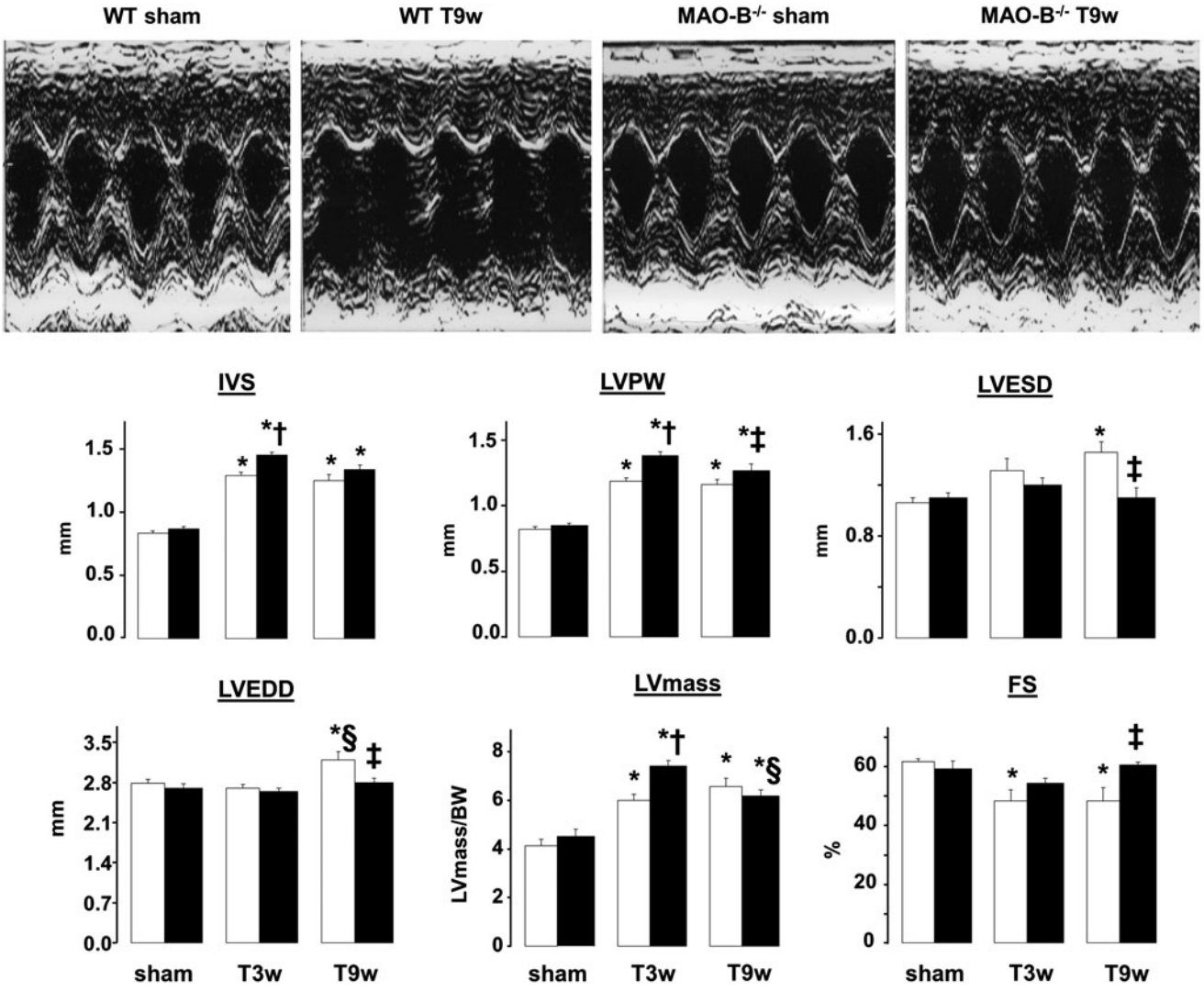

FIG. 1. Changes in cardiac morphology and function in sham-operated and pressure overloaded WT and MAO-B$^{-/-}$ mice. Representative M-mode echocardiographic images (*upper panel*). Changes in cardiac morphology and function in WT ($n = 7$, *white bars*) and MAO-B$^{-/-}$ mice ($n = 8$, *black bars*) after 3 and 9 weeks of TAC. *$p < 0.05$ *versus* respective sham, $^{\dagger}p < 0.05$ *versus* WT T3w, $^{\ddagger}p < 0.05$ *versus* WT T9w, $^{\S}p < 0.05$ *versus* respective T3w. MAO, monoamine oxidase; TAC, transverse aortic constriction; WT, wild type; IVS, interventricular septum; LVPW, left ventricular posterior wall; LVESD, left ventricular end-systolic dimension; LVEDD, left ventricular end-diastolic dimension, left ventricular mass normalized to body weight (LVmass/BW, expressed as mg of left ventricle/gram of body weight); FS, fractional shortening; T3w, TAC 3 weeks; T9w, TAC 9 weeks.

MAO-B$^{-/-}$ mice display fully preserved LV function when subjected to chronic pressure overload

Next, we conducted an *in vivo* assessment of load-independent LV function and hemodynamics *via* pressure-volume (PV) relationships. As displayed in Figure 2, dP/dt_{max} and dP/dt_{min} were lower in MAO-B$^{-/-}$ mice compared to WT littermates at baseline. Preload-recruitable stroke work, a load-independent index of systolic function derived from PV data (13) showed a borderline significant decline ($p = 0.053$). End-diastolic volume (EDV), end-systolic volume (ESV), and ejection fraction (EF) were not statistically different between the two groups.

When subjected to pressure-overload, WT, and MAO-B$^{-/-}$ mice behaved very differently. By 9 weeks of TAC, WT hearts dilated more, and exhibited a right-ward shift in the PV loops, consistent with maladaptive remodeling and worsened systolic function (Fig. 2A). Both EDV and ESV were larger in controls, with a fall in EF that was not observed in MAO-B$^{-/-}$ mice. Directionally opposite changes in indexes of systolic function were observed, with declines in controls and improvement in MAO-B$^{-/-}$. Thus, despite having a slight reduction of basal function, MAO-B$^{-/-}$ hearts were resistant to adverse LV dilation and dysfunction from pressure overload.

Dopamine catabolism is enhanced in failing hearts, while MAO-B deletion prevents oxidative stress and reactive aldehyde formation

We assessed MAO-B expression and dopamine catabolism in mice subjected to pressure overload *via* TAC. Although MAO-B protein expression was unchanged in cardiac tissue

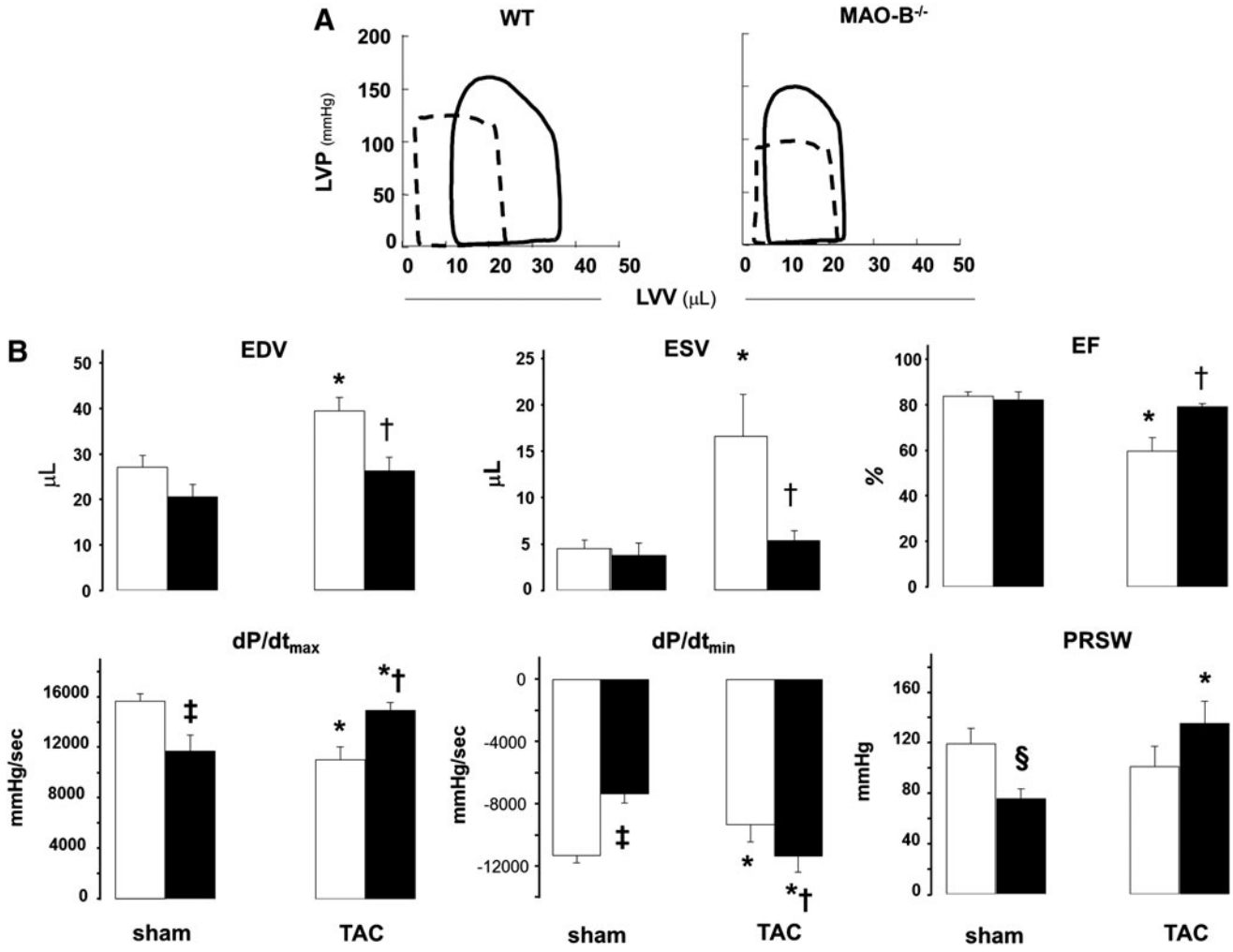

FIG. 2. PV relationships in WT and MAO-B$^{-/-}$ mice. (A) Representative PV loops from WT and MAO-B$^{-/-}$ at baseline (*dashed line*) and 9 weeks after TAC (*full line*). **(B)** Morphological and functional changes determined *via* PV relationships in WT (*white bars*) and MAO-B$^{-/-}$ (*black bars*) mice at baseline ($n=6$ each group) and after 9 weeks of TAC ($n=8$ each group). $^{*}p<0.05$ *versus* sham, $^{\dagger}p<0.01$ *versus* WT T9w, $^{\ddagger}p<0.01$ *versus* WT sham, $^{\S}p=0.053$ *versus* WT sham. LVP, left ventricular pressure; LVV, left ventricular volume; PV, pressure-volume; EDV, end-diastolic volume; ESV, end-systolic volume; EF, ejection fraction; dP/dt$_{max}$, an index of myocardial contractility; dP/dt$_{min}$, an index of relaxation; PRSW, preload-recruitable stroke work, index of contractility.

after 9 weeks of TAC (Fig. 3A), we found that dopamine levels were markedly reduced (Fig. 3B). Interestingly, the ratio between DOPAC, a dopamine catabolite downstream of MAO-B activity, and dopamine was ostensibly increased (Fig. 3B). This finding suggests that MAO-B activity is upregulated in hearts subjected to TAC, likely owing to higher substrate availability and resulting in augmented intracardiac levels of the byproducts of its activity. Considering that MAO-B activation results in formation of hydrogen peroxide and reactive aldehyde intermediates, we assessed the oxidative stress and aldehyde levels and whether lack of MAO-B can affect their accumulation. Levels of 4-hydroxynonenal (4-HNE), a product of lipid peroxidation, were significantly increased in WT hearts subjected to TAC, but not in MAO-B$^{-/-}$ hearts (Fig. 3C). On one hand, this suggests that levels of oxidative stress are reduced in the absence of MAO-B. On the other, it also shows that aldehyde formation is enhanced in WT hearts subjected to TAC, most likely because ALDH2 activity is not sufficient to clear the excessive formation of aldehyde intermediates.

Both apoptosis and fibrosis are reduced in MAO-B$^{-/-}$ mice

Histological data presented in Figure 4A confirmed echo-data by showing that the left ventricle was enlarged in WT mice subjected to TAC. Such change was absent in MAO-B$^{-/-}$ suggesting that the loss of viable cardiomyocytes might be responsible for the enlarged chamber volumes. Furthermore, since myocyte cross-sectional diameter did not change in both WT and MAO-B$^{-/-}$ mice (Fig. 4B), it is possible that the accumulation of excess collagen is also responsible, at least, in part, for altered LV dimensions.

To assess whether the absence of MAO-B results in a more viable myocardium after pressure overload, we measured levels of apoptosis in failing hearts (14, 41). As expected, after 9 weeks of TAC WT hearts showed an increased number of terminal deoxynucleotidyl transferase dUTP nick end labeling (TUNEL) positive nuclei. Conversely, such rise did not occur in MAO-B$^{-/-}$ hearts (Fig. 5A). As

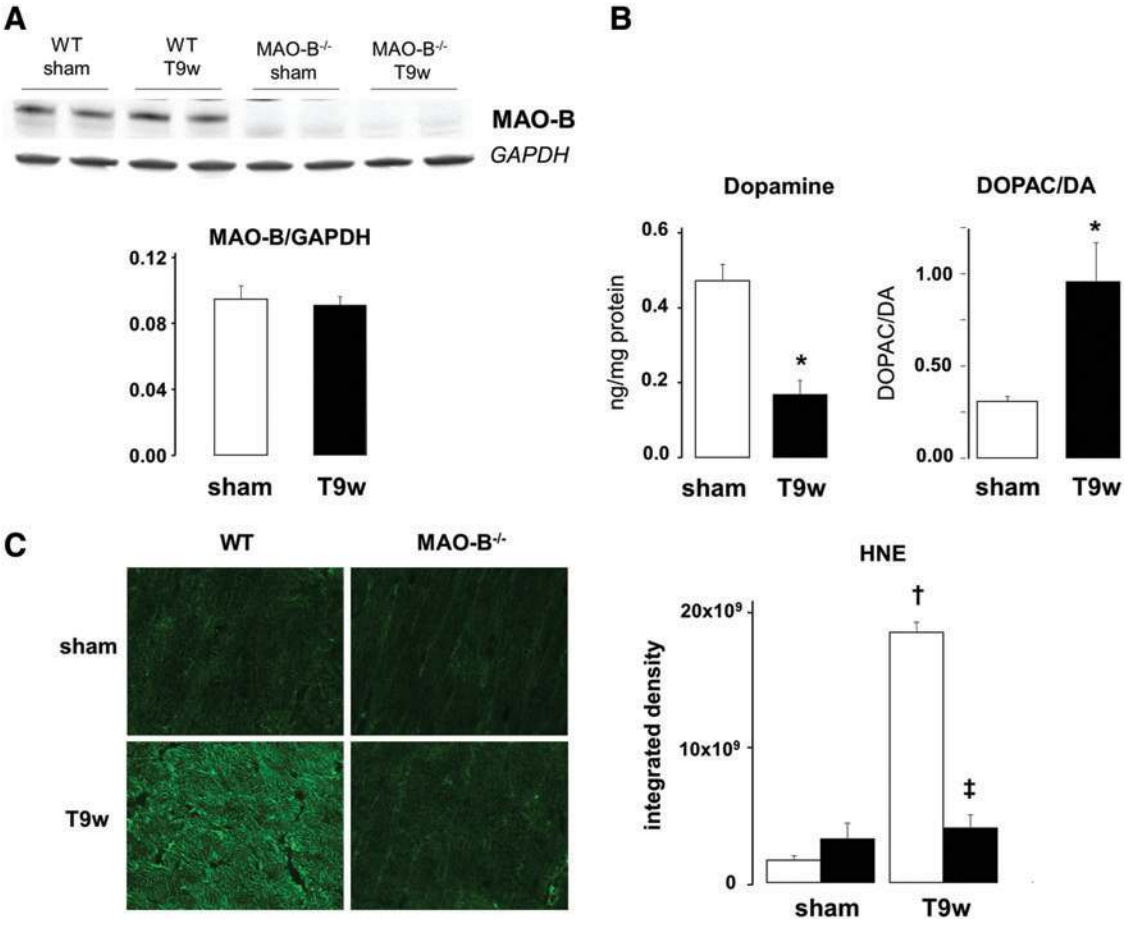

FIG. 3. Dopamine (DA) catabolism, oxidative stress and aldehyde levels in WT and MAO-B$^{-/-}$ mouse hearts after pressure overload. (A) MAO-B protein expression in sham-operated and 9 weeks TAC WT and MAO-B$^{-/-}$ mice. **(B)** DA levels (*left*) in the myocardium of sham-operated and 9 weeks TAC (T9w) mice and DOPAC to DA ratio (*right*) as an index of DA catabolism in sham-operated and 9 weeks TAC mice. **(C)** Levels of 4-hydroxynonenal (4-HNE) in cryosections from sham-operated ($n=4$) and 9 weeks TAC WT ($n=4$, *white bars*) and MAO-B$^{-/-}$ mice ($n=4$, *black bars*). *$p<0.05$, $^{\dagger}p<0.001$ *versus* sham, $^{\ddagger}p<0.001$ *versus* WT T9w. DOPAC, 3,4-dehydroxyphenylacetic acid. To see this illustration in color, the reader is referred to the web version of this article at www.liebertpub.com/ars

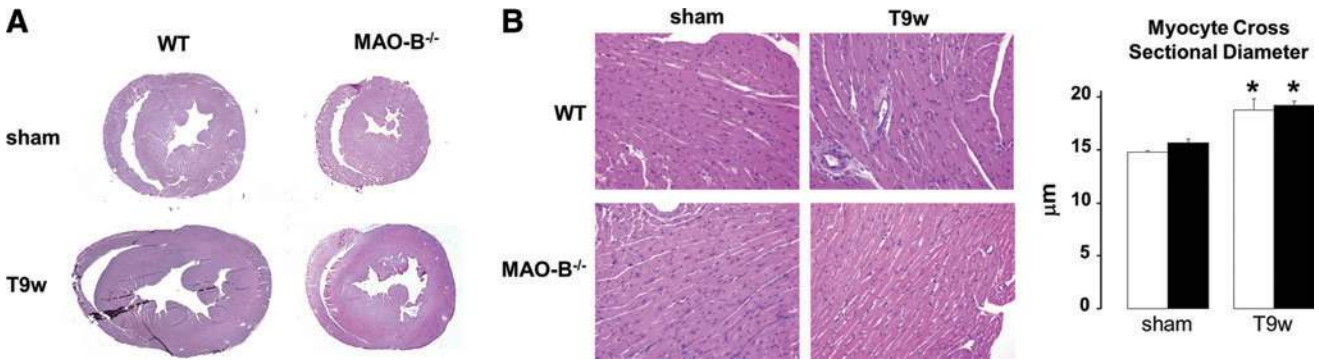

FIG. 4. Lack of MAO-B prevents chamber dilation but not hypertrophy. (A) Examples of transversal left ventricle sections from sham operated and 9 weeks TAC (T9w) WT and MAO-B$^{-/-}$ mice. **(B)** Representative images (*left*) of H&E stained cardiac sections show cardiomyocytes hypertrophy (quantified on the right). WT: *white bars* ($n=5$), MAO-B$^{-/-}$: *black bars* ($n=5$). *$p<0.05$ *versus* respective sham. To see this illustration in color, the reader is referred to the web version of this article at www.liebertpub.com/ars

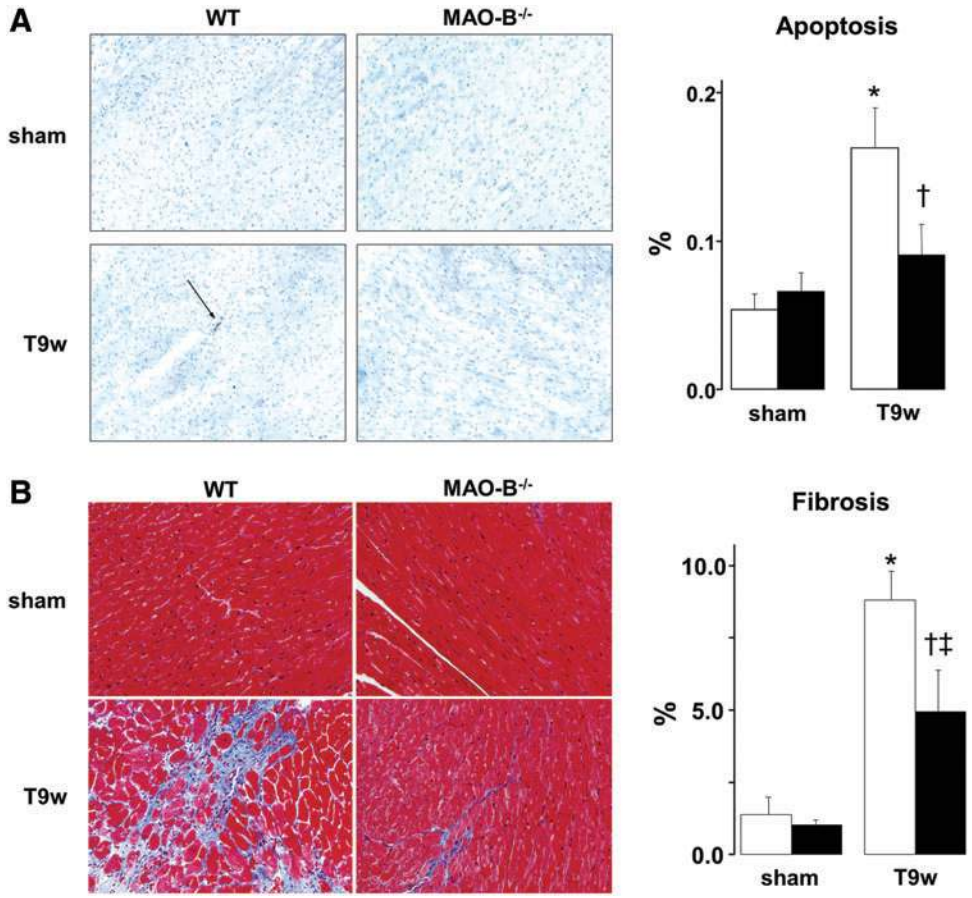

FIG. 5. Apoptosis and fibrosis are reduced after pressure overload in mice lacking MAO-B. (A) Representative images of TUNEL staining in sections from WT (*white bars*) and MAO-B$^{-/-}$ mice (*black bars*) at baseline ($n=5$, sham) and after 9 weeks of pressure overload ($n=8$, T9w). *Arrows* indicate TUNEL positive nuclei, quantified in the graph on the right. **(B)** Masson's Trichrome stained myocardium from WT and MAO-B$^{-/-}$ mice before ($n=5$) and after pressure overload ($n=8$). Blue color reflects fibrosis (quantified on the right). *$p<0.005$ *versus respective sham*, †$p<0.05$ *versus* WT T9w, ‡$p<0.001$ *versus* WT sham. WT, wild type; TUNEL, terminal deoxynucleotidyl transferase dUTP nick end labeling. To see this illustration in color, the reader is referred to the web version of this article at www.liebertpub.com/ars

previously observed in this mouse heart failure model (25, 37), fibrosis was very prominent in WT TAC hearts (Fig. 5B). However, its levels were markedly reduced in MAO-B$^{-/-}$ hearts.

Extracellular signal regulated kinase 1/2 phosphorylation is increased in MAO-B$^{-/-}$ mice

Since extracellular signal regulated kinase (ERK) activation is involved in cardiac myocyte growth and contractility, we assessed its status also in these mice. We found that, when compared to WT mice, ERK1/2 was more phosphorylated in MAO-B$^{-/-}$ mice after 9 weeks of pressure overload (Fig. 6). This finding suggests that compensated hypertrophy observed in MAO-B$^{-/-}$ mice might be supported by enhanced ERK activation (8, 14).

MAO activation directly jeopardizes mitochondrial function in myocytes by enhancing ROS emission

Mitochondrial function is profoundly altered in failing hearts (24). Since MAOs are located in the mitochondria, we hypothesized that MAOs activation can directly perturb mitochondrial functional assets. To test this novel idea, ROS formation and mitochondrial membrane potential were assessed in neonatal and adult cardiomyocytes. We transfected neonatal cardiomyocytes with HyPer, a genetically encoded fluorescent hydrogen peroxide sensor that can be targeted to several intracellular compartments. In particular, we used HyPer$_{mito}$ which is targeted specifically to the mitochondria of cardiomyoctes (Fig. 7A). When these cells were treated with MAO-B substrate dopamine, this resulted in increased mitochondrial hydrogen peroxide production as per increased HyPer$_{mito}$ fluorescence ratio (Fig. 7A). This rise was completely prevented by MAO inhibitor pargyline. Since dopamine was used as the substrate, hydrogen peroxide production can be entirely ascribed to MAO-B activation. To assess whether there is a difference in the hydrogen peroxide formation at the mitochondrial *vs*. the cytosolic level, we used cytosol targeted HyPer (HyPer$_{cytosol}$). This probe shows typically diffused cytosolic distribution and is responsive to exogenously added H_2O_2 (Supplementary Fig. S2A). We then compared the time-course of redox changes between myocytes expressing HyPer in these two compartments, and found that the fluorescence ratio of HyPer$_{mito}$ started to increase after only 10 min of dopamine addition, whereas the HyPer$_{cytosol}$ fluorescence ratio increased only after 30 min (Supplementary Fig. S2B).

These observations were validated in adult cardiomyocytes isolated from WT and MAO-B$^{-/-}$ mice cultured in presence of dopamine. Using Mitotracker Red CM-H_2XRos, we show that ROS formation is significantly higher in WT cardiomyocytes when compared to ones lacking MAO-B (Fig. 7B). Same experiments were performed in parallel in neonatal cardiomyocytes (Supplementary Fig. S2C) using Mitotracker Red CM-H_2XRos and showed that both HyPer$_{mito}$ and Mitotracker Red CM-H_2XRos can detect mitochondrial ROS generation. Taken together, these results suggest that MAO-B

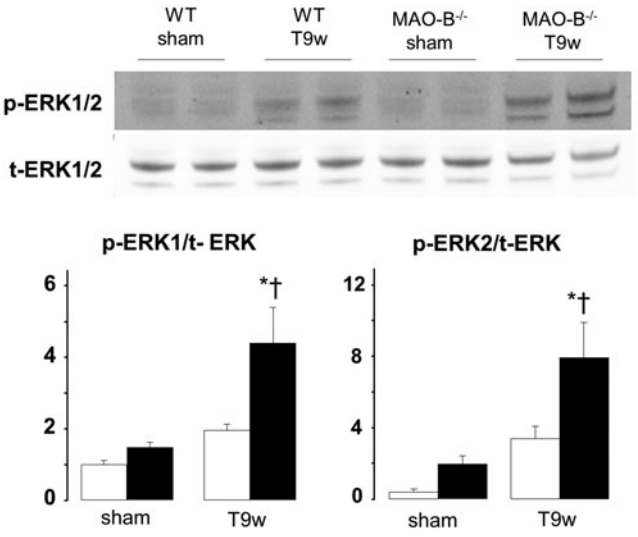

FIG. 6. ERK1/2 activation in WT and MAO-B$^{-/-}$ mice subjected to pressure overload. Western blots for phospho- and total-ERK1/2 (*upper panel*) and densitometric analysis (*lower panel*). WT, wild type. WT: *white bars* ($n=5$), MAO-B$^{-/-}$: *black bars* ($n=6$). *$p<0.01$ *versus* sham, $^{\dagger}p<0.05$ *versus* WT T9w. ERK1/2, extracellular signal regulated kinase 1/2.

activation augments H_2O_2 formation mainly at the mitochondrial level, both in neonatal and adult cardiomyocytes.

It is pathophysiologically relevant to establish whether MAO activation may directly alter mitochondrial bioenergetic assets. To test this idea, we used tetramethylrhodamine methyl ester (TMRM) to measure mitochondrial membrane potential, in the absence and presence of ATP synthase inhibitor oligomycin (Fig. 8A). Normally, the proton gradient generated by the electron transport chain is used at the level of ATP synthase to promote ATP formation. However, when the electron transfer chain is not functional, ATP synthase may start operating in reverse, hydrolyzing ATP while extruding protons to maintain membrane potential. This mechanism of compensation can be unmasked after ATP synthase inhibition with oligomycin, because under these conditions cells that hydrolyze glycolytically synthesized ATP would immediately loose membrane potential (23). There was no difference in mitochondrial membrane potential between vehicle or dopamine treated neonatal cardiomyocytes (Fig. 8B). In stark contrast, when cells were coincubated with dopamine and ATP synthase inhibitor oligomycin, membrane potential dropped by ~50%. The MAO-B inhibitor pargyline offset this change suggesting that MAO activation induces a latent mitochondrial dysfunction, causing mitochondria to hydrolyze ATP (Fig. 8B, Supplementary Fig. S3). These same findings were reproduced in adult cardiomyocytes isolated from WT and MAO-B$^{-/-}$ mice, although with a slightly different time-course. Adult WT cardiomyocytes started to depolarize 20 min after the addition of oligomycin and dopamine, and they were completely depolarized 45 min later (Fig. 8C). Conversely, in neonatal myocytes a longer incubation (3 h) was required to see the same phenomenon, most likely due to the significantly higher expression of MAO-B in adult cardiomyocytes. These alterations were not observed in MAO-B$^{-/-}$ myocytes (Fig. 8C); thus, further confirming that persistent MAO-B activation can directly target mitochondrial function.

Aldehyde intermediates generated by MAO-B also contribute to alter mitochondrial function

Our *in vivo* studies suggest that toxic and reactive aldehydes are accumulated in pressure overloaded hearts. Hence, we hypothesized that aldehydes deriving from MAO activity could also affect mitochondrial function and ultimately lead to cell death. To directly test this possibility, we first inhibited the activity of ALDH, a dopamine catabolic enzyme downstream of MAO, through a pharmacological approach using cyanamide. Dopamine addition to cardiomyocytes pretreated with cyanamide resulted in a 50% loss in membrane potential (Fig. 9A), whereas pargyline obviated this change completely. To further confirm this finding and to identify the main ALDH isoform implicated in this phenomenon, we used a more specific, siRNA-based approach against ALDH2. After 24 h of siRNA treatment, we obtained a maximal 50% reduction in ALDH2 protein expression (Fig. 9B). In these siRNA treated cells, dopamine caused a 40% reduction in mitochondrial membrane potential (Fig. 9C). MAO inhibition *via* pargyline completely prevented this drop. Taken together, these results suggest that aldehyde intermediates deriving from MAO activity can directly target mitochondria, leading to organelle dysfunction.

Discussion

This study shows that lack of MAO-B prevents LV dilation and functional decompensation in hearts subjected to pressure overload. This assertion is grounded in present evidence showing that MAO-B activation appears to produce several major adverse effects. Here we show for the first time that inhibiting MAO-B results in reduced formation of H_2O_2 and aldehydes which otherwise can synergize to cause mitochondrial dysfunction. Our study also highlights that ALDH2 may play an important role in heart failure, mimicking its adverse contribution to I/R injury and diabetic cardiomyopathy (11, 44).

Impact of MAO-B deletion on LV adaptation to chronic stress conditions

We recently demonstrated that pharmacological inhibition or genetic ablation of MAO-A counteracts adverse remodeling and contractile failure in hearts subjected to pressure overload (25). MAO-A activity is central to the enhanced norepinephrine catabolism present in the failing hearts. Differently from MAO-A, the possible pathogenetic contribution of MAO-B to heart failure has been completely neglected despite the fact that this isoenzyme is highly expressed in mouse and human hearts (15, 27, 36) and its pivotal role in dopamine degradation in the brain of human and other primates (7). Here we report that the genetic ablation of MAO-B favors the maintenance of stable concentric hypertrophy with maintained LV function, preventing the transition to overt LV dilation and pump failure in pressure overloaded hearts. Our data suggest that this is most likely due to enhanced dopamine degradation by MAO-B that, in turn, leads to elevated oxidative stress and aldehyde accumulation. Although MAO-B expression was not altered in TAC hearts, we show that increase in its activity is due to higher substrate availability, as previously reported also for MAO-A in heart failure (25). We furthermore found that ERK1/2 is upregulated in TAC MAO-B$^{-/-}$. These findings dovetail nicely with the

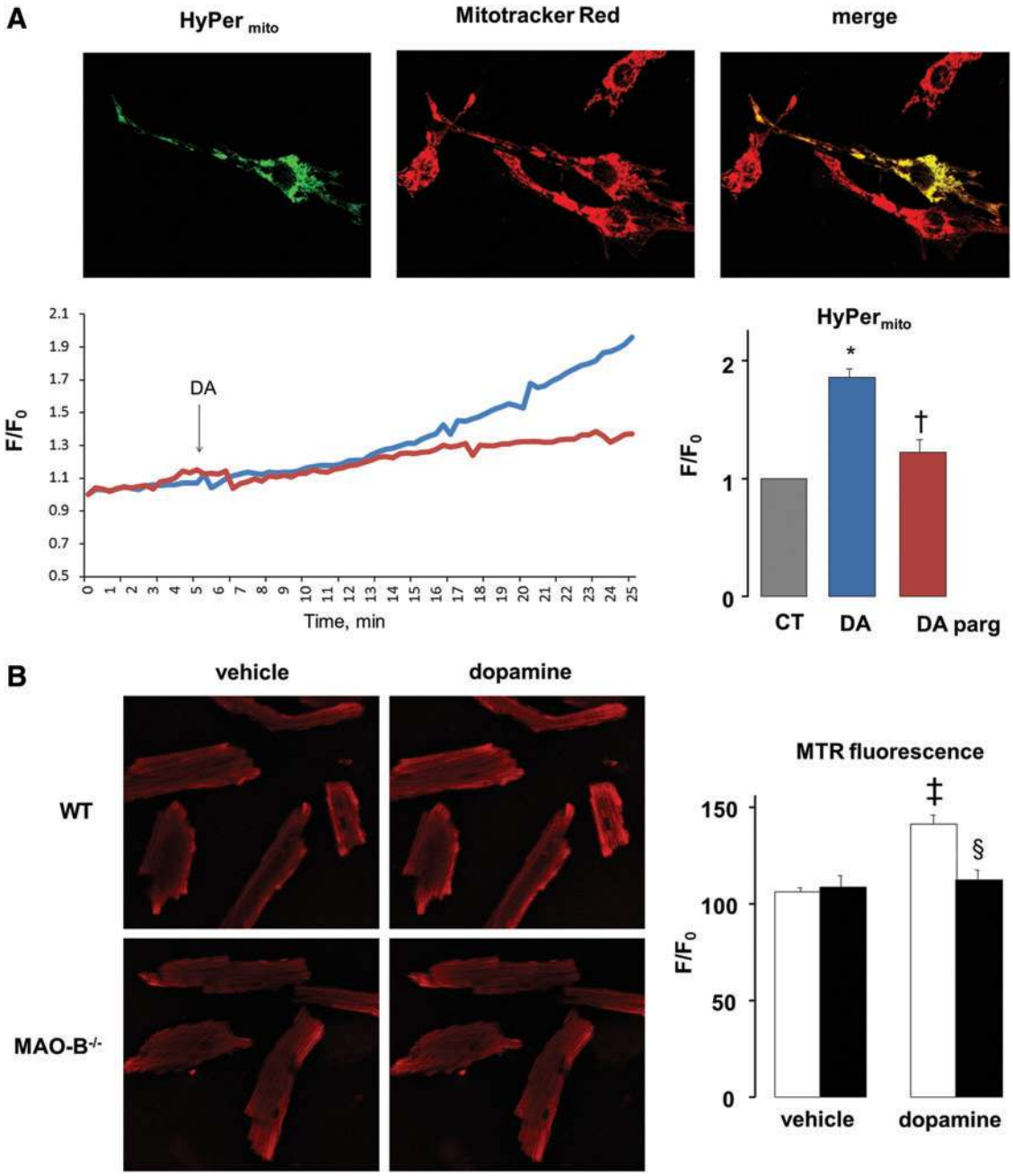

FIG. 7. Effects of MAO activation on mitochondrial ROS generation. (A) Images showing cell transfected with mitochondria-targeted HyPer ($HyPer_{mito}$), stained with mitochondrial dye Mitotracker Red and their overlap. Graph on the left shows $HyPer_{mito}$ fluorescence ratio change with time after DA addition without (blue line) or with (red line) pargyline (parg). Graph on the right shows mitochondrial ROS production determined by mitochondria-targeted Hyper 30 min after DA addition. **(B)** Adult cardiomyocytes isolated from WT and MAO-$B^{-/-}$ mice stained with Mitotracker Red CM-H_2XRos (MTR) before and after the addition of DA (*left panel*). MTR fluorescence intensity ratio is quantified on the right. WT: *white bars*, MAO-$B^{-/-}$: *black bars*. *$p<0.05$ *versus* control, $^{\dagger}p<0.05$ *versus* DA, $^{\ddagger}p<0.001$ *versus* WT vehicle, $^{\S}p<0.005$ WT DA *versus* MAO-$B^{-/-}$ DA. CT, control; ROS, reactive oxygen species; WT, wild type; F/F_0, fluorescence intensity relative to resting fluorescence. To see this illustration in color, the reader is referred to the web version of this article at www.liebertpub.com/ars

consolidated knowledge attesting MEK1-ERK1/2 signaling cascade as a master regulator of physiological hypertrophy. Activated MEK1 promotes specific activation of ERK1/2 resulting in preserved or even increased cardiac function in stressed hearts (8). Interestingly, the inhibition of ERK1/2 in TAC hearts predisposes the myocardium to decompensation associated with greater apoptosis rates (26, 33). Although the mechanisms whereby ERK1/2 might directly protect cardiac myocytes from cell death remain to be elucidated in full, a link between ERK, the transcription factor GATA4 and the activation of the antiapoptotic gene *Bcl-X 2* has been suggested to explain cardiac cell survival under disease conditions, such as that imposed by drug-induced cardiotoxicty (2, 26). At this stage, our data remain correlative, but ongoing efforts in our

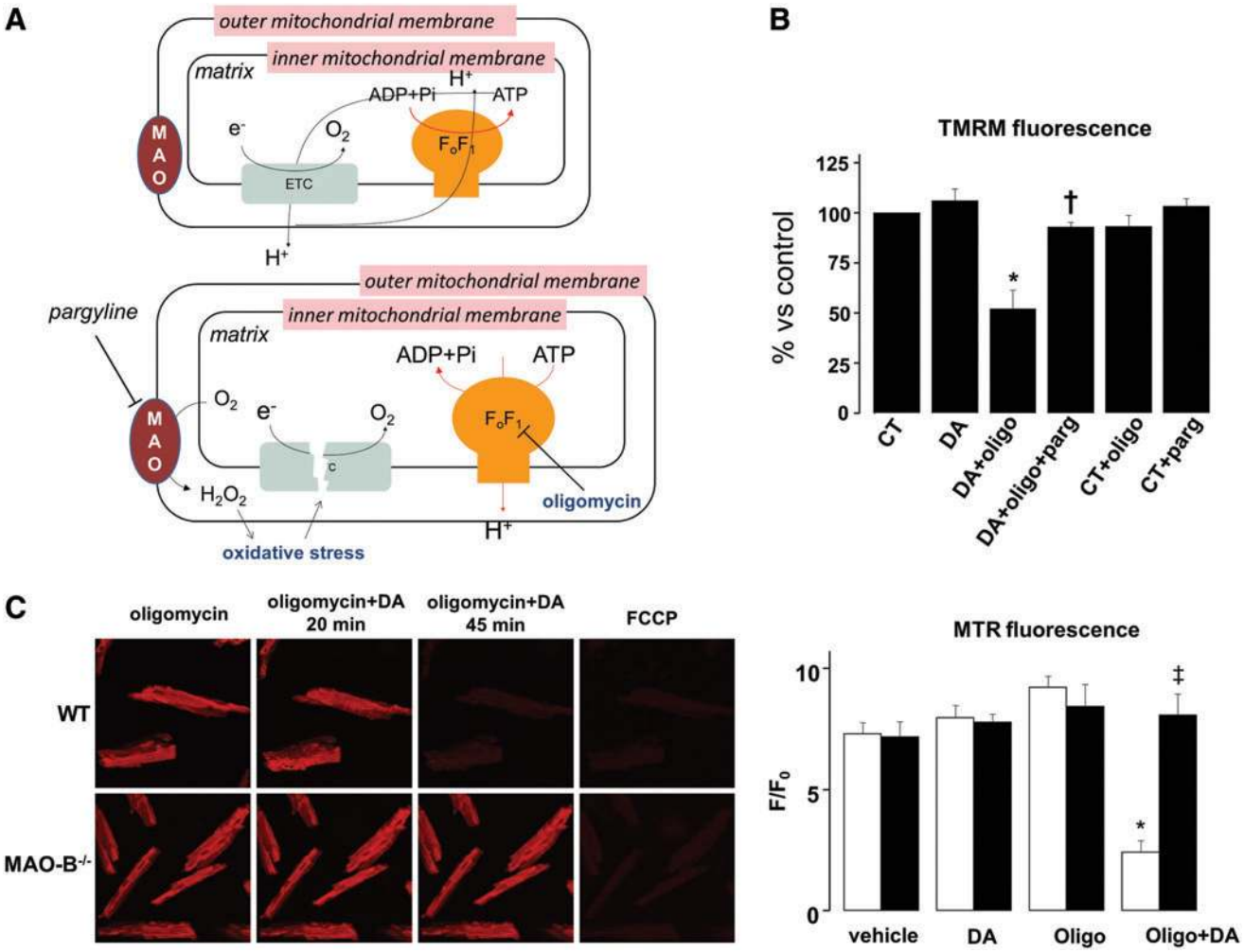

FIG. 8. Effects of MAO activation on mitochondrial function. (A) Mechanism of action of oligomycin. In normal conditions (*upper panel*), electrons are transferred across the respiratory chain with concomitant extrusion of protons at the level of complexes I, III, and IV which generates membrane potential. This proton gradient is used at the level of ATP synthase to promote ATP formation. However, when the electron transfer chain is dysfunctional (*lower panel*), ATP synthase may start working in reverse, hydrolyzing ATP and extruding protons to maintain membrane potential. In the presence of ATP synthase inhibitor oligomycin, this mechanism of compensation can be unmasked, since cells which hydrolyze glycolytically synthesized ATP immediately loose membrane potential. **(B)** Mitochondrial membrane potential in neonatal cardiomyocytes after 3 h of incubation with DA, oligomycin and without or with pargyline. **(C)** Mitochondrial membrane potential in adult cardiomyocytes isolated from WT (*white bars*) and MAO-B$^{-/-}$ (*black bars*) mice and exposed to DA and oligomycin. *$p < 0.05$ *versus* DA, $^{\dagger}p < 0.07$ *versus* DA + oligo, $^{\ddagger}p < 0.05$ *versus* WT oligo + DA. WT, wild type; F/F_0, fluorescence intensity relative to resting fluorescence; FCCP, carbonyl cyanide 4-(trifluoromethoxy)phenylhydrazone; TMRM, tetramethylrhodamine methyl ester. To see this illustration in color, the reader is referred to the web version of this article at www.liebertpub.com/ars

lab aim at exploring this possibility in full, using both isolated myocytes and TAC mice.

MAO-B activity through ROS and aldehydes contribute to alter mitochondrial function

Mitochondrial dysfunction is frequently associated with oxidative stress and cell death leading, in turn, to heart failure. However, the modalities of this complex interplay are not fully understood yet. Here we deepened our understanding of how ROS, MAO, and dopamine (and likely other catecholamines) are intermingled. Indeed, we showed that activating MAO *in vitro* led to increased oxidative stress and mitochondrial dysfunction. We were able to compartmentalize and follow the time-course of ROS formation after MAO activation. Use of the genetically encoded redox sensitive fluorescent probe HyPer enabled us to target it specifically to mitochondria or cytosol, demonstrating that H_2O_2 formation occurs much earlier at the mitochondrial level rather than in the cytosol. This is an important finding because it reiterates the issue that mitochondria could be the first and likely one of the primary targets of endogenously produced H_2O_2 and associated adverse ROS signaling, eventually leading among others to oxidative damage to mitochondrial DNA (21). However, this dysfunction was latent and could be uncovered only after incubation with oligomycin, indicating that ATP synthase is working in the reverse mode, that is, hydrolyzing glycolytically generated

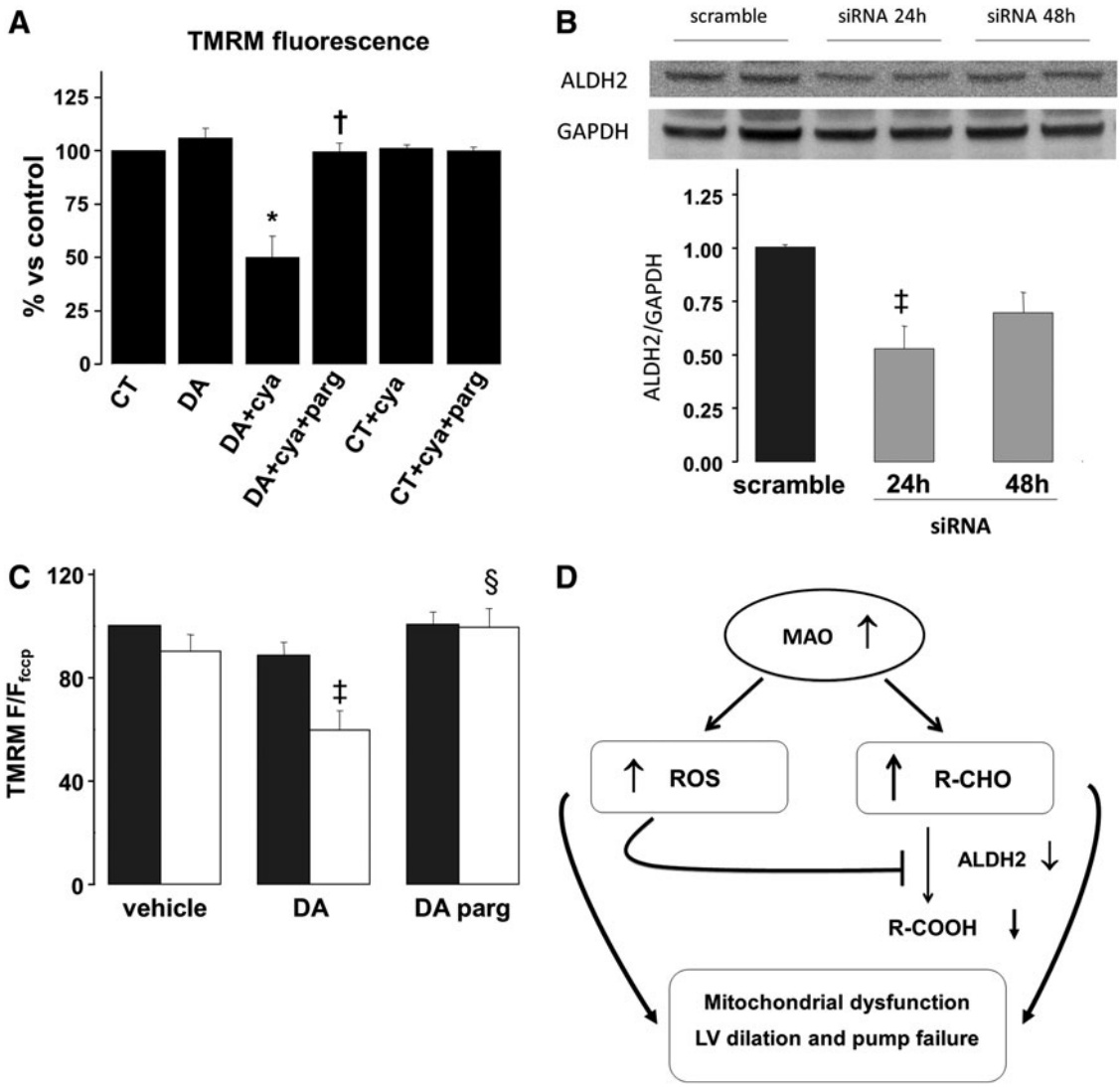

FIG. 9. Effects of concomitant MAO activation and ALDH inhibition on mitochondrial function. (A) Mitochondrial membrane potential after 3 h of incubation with DA, aldehyde dehydrogenase (ALDH) inhibitor cyanamide (cya) and without or with pargyline (parg). **(B)** ALDH2 expression in neonatal cardiomyocytes after 24 or 48 h of ALDH2 siRNA treatment. **(C)** Mitochondrial membrane potential in scramble RNA treated cells (*dark grey bars*) and ALDH2 siRNA treated cells (*white bars*) after incubation with DA, in the absence or presence of pargyline. **(D)** Scheme depicting possible effects of products deriving from MAO activation. Increased ROS generation can inhibit the activity of ALDH2 which may, in turn, cause the accumulation of toxic aldehydes deriving from amine catabolism. Both ROS and aldehydes may induce mitochondrial dysfunction and contribute to myocardial damage. $^{*}p < 0.001$ *versus* CT, $^{\dagger}p < 0.005$ *versus* DA + cya, $^{\ddagger}p < 0.05$ *versus* CT scramble, $^{\S}p < 0.05$ *versus* DA ALDH2 siRNA. F/F_{fccp}, fluorescence normalized to fluorescence; F/F_0, fluorescence intensity relative to resting fluorescence; FCCP, carbonyl cyanide 4-(trifluoromethoxy)phenylhydrazone; TMRM, tetramethylrhodamine methyl ester.

ATP and compensating in this way for the dysfunctional respiratory chain (23).

Another interesting aspect is the cardiac accumulation of aldehydes and the possibility that also MAO-derived aldehydes may contribute to cardiac damage. In the heart, these chemical species are normally rapidly inactivated and transformed into corresponding acids by ALDH2, the most abundant ALDH isoform expressed in this tissue and localized in the mitochondria (1). However, high oxidative stress, such as that occurring after I/R or in heart failure may trigger lipid peroxidation and accumulation of reactive aldehydes, namely 4-HNE and malondialdehyde (11, 25). Aldehydes inactivate a number of macromolecules, including the proteasome, the electron transport chain in the mitochondria, as well as ALDH2 itself (12). Indeed, treatment with ALDH2 activator Alda-1 increased ALDH2 activity by two-fold and reduced infarct size by 60% in an *in vivo* model of myocardial infarction in rats (11). Although no direct evidence is available yet, our current data showing increased levels of the ALDH2 substrate 4-HNE in our *in vivo* TAC hearts suggest that ALDH2 activity might be reduced in heart failure, whereas aldehyde formation might be enhanced. Mitochondrial membrane potential dropped when cardiomyocytes expressing 50% less ALDH2 were incubated with MAO-B substrate dopamine, likely owing to DOPAL accumulation. The latter is an aldehyde deriving

from dopamine that is known to be very reactive and a potent neurotoxin (9). Along this same line, other MAO substrates, such as norepinephrine, can also be transformed into aldehyde intermediates, but testing their toxicity and reactivity in the context of chronic cardiac diseases requires further investigation. Altogether, this set of data lends support to the novel hypothesis that, mitochondria are targets of MAO-generated ROS and aldehyde intermediates that, in turn, can further fuel mitochondrial and myocardial damage (Fig. 9D).

Limitations, translational impact and conclusions

The major limitation to this work is the observation that MAO-B$^{-/-}$ mice have slightly altered basal cardiac function and likely β-adrenergic desensitization, accounting for possible lower vascular resistance. While addressing this question warrants fully-dedicated studies, the present report unequivocally indicates that, in face of this lower initial performance, MAO-B$^{-/-}$ mice cope better with stress, where the absence of MAO-B prevents oxidative stress, LV dilation and pump failure. This issue could be addressed using conditional, cardiomyocyte-specific overexpressing or null MAO-A or -B mice that are currently not available. These mice would also make it possible to answer another important translational question in perspective, that is, whether deleting either MAO-A or -B or both can actually reverse LV remodeling and dysfunction once the insult is already instituted. Future studies are also needed to elucidate the biochemical and functional links between MAO and ERKs, as well as the ability of MAO deletion to prevent mitochondrial ROS generation and dysfunction after pressure overload, thereby resulting in maintained ATP levels.

Present studies may have translational implications in several clinical settings. These include (but are not limited to) congestive heart failure, diabetes and hypertension. Indeed, elevated plasma norepinephrine levels and increased spillover of norepinephrine into the plasma in heart failure are mainly due to decreased efficiency of norepinephrine reuptake by sympathetic efferent fibers (22, 28, 30). Interestingly, the extraneuronal norepinephrine uptake in heart failure patients is almost doubled (17). Furthermore, also, diabetes may be characterized by increased cardiac sympathetic tone, thought to contribute to myocardial injury, and is accompanied by augmented oxidative stress in type 1 diabetes patients (29, 32). Changes in mitochondrial energetic and redox assets take center stage also in this syndrome. Thus, present findings provide initial, critical groundwork to establish whether MAO-B inhibitors merit consideration for clinical testing in patients suffering from these syndromes.

Materials and Methods

Animals and procedures

MAO-B$^{-/-}$ mice and their WT littermates in 129/Sv background were used ($n=22$). MAO-B$^{-/-}$ mice were generated as previously described (20). TAC was performed following a previously reported protocol (40). After induction of anesthesia and intubation, mice were placed on a volume ventilator (120 breaths/min, 1.2 ml/g/min) and anesthesia was maintained with 5% isofluorane. The aortic arch was isolated and tied against a 27-gauge needle, resulting in a 65%–70% constriction after the removal of the needle. The chest and skin were closed and animals extubated and allowed to fully recover. Sham-operated mice underwent the same operation except that after the aortic arch was isolated, no ligature was placed. The Johns Hopkins University Institutional Animal Care and Use Committee approved all animal experiments, which conformed to the guidelines of the National Institutes of Health.

Echocardiography

In vivo cardiac morphology and function were assessed by serial M-mode echocardiography (Acuson Sequioa C256, 13 MHz transducer; Siemens) performed in conscious mice. LV end-systolic and end-diastolic dimensions were averaged from 3–5 beats. LV percent FS and LV mass were calculated as described previously (38). Thickness of posterior free wall and IVS were averaged.

In vivo *hemodynamics*

In vivo cardiac function was assessed by PV catheter in anesthetized mice employing a four-electrode PV catheter (model SPR-839; Millar Instruments) as previously described (19). Anesthesia was maintained with i.p. etomidate (250 μg), urethane (30 mg) and morphine (15 μg). Mouse was placed in supine position on a thermoregulated surgical table maintained at 37°C. Ventilation *via* endotracheal tube was maintained with 100% oxygen using a custom-designed constant flow ventilator delivering a tidal volume of 6.7 μl/g at 120 breaths/min. An internal jugular venous line was placed to provide a fluid and drug delivery port. The thorax was opened and a miniature PV catheter inserted into the LV *via* the apex for continuous LV PV data. Calibration of the signal was performed using injection of hypertonic saline and direct measurement of cardiac output *via* an aortic flow probe (Transonic Instruments) placed around thoracic descending aorta. PV loop analysis was made using a custom analysis program (WinPVAN 3.3).

Immunohistochemistry for 4-HNE-modified proteins

LV cryosections were blocked in 10% goat serum PBS for 1 h at room temperature. Next, the sections were incubated with the anti-4-HNE (1:5; Abcam, ab48506) antibody in 5% goat serum PBS overnight at 4°C. After washing, AlexaFluor488 secondary antibody (Invitrogen) was incubated for 30 min at room temperature, and then visualized by confocal microscopy (Zeiss; LSM 510 Meta). For negative control experiments, primary antibody was omitted. Images were analyzed using computer-assisted image analysis systems (ImageJ; NIH).

Histology

Hearts were fixed in 10% formalin overnight, embedded in paraffin, sectioned at 5 μm thickness, and stained using H&E and Masson's trichrome (25). Photomicrographs of the sections were evaluated for myocyte cross-sectional diameter and interstitial collagen fractions using computer-assisted image analysis systems (Adobe Photoshop).

Apoptosis detection by TUNEL staining

The assay was performed using a commercially available kit according to manufacturer's instructions (ApopTag;

Millipore). TUNEL-positive and methyl green counterstained nuclei were visualized using a light microscope equipped with a camera. The percentage of TUNEL-positive cardiomyocytes is expressed as a percentage of total nuclei.

Neonatal rat cardiomyocytes studies

Myocytes were isolated from 1–2 days old Sprague Dawley rats, as previously described (37). After 2 days of culture, myocytes were pretreated with 100 μM pargyline for 30 min, and then subjected to stimulation with dopamine for 2 h (1.5 μM). For mitochondrial ROS production measurements, cells were loaded with the reduced form of Mitotracker Red (100 nM, Mitotracker Red CM-H_2XRos, Molecular probes) for 30 min at 37°C, washed, and then analyzed and images acquired by fluorescent microscopy. For the mitochondrial membrane potential measurements, cells were loaded with 25 nM TMRM for 30 min at 37°C, and then analyzed as before. For the experiments employing oligomycin, after 2 h incubation with dopamine, cells were incubated with oligomycin 6.3 μM for another hour at 37°C, and then loaded with TMRM and analyzed. Images were analyzed and fluorescence intensities determined using computer-assisted image analysis systems (ImageJ; NIH). Approximately 100–150 cells were analyzed per condition in each experiment. All the experiments were repeated at least thrice.

Transfection

Neonatal rat cardiomyocytes were plated on six-well plates at a density of 4×10^5 cells/well and transfected with Lipofectamine reagent (Invitrogen). For each transfection, 3 μg of plasmid ($HyPer_{mito}$ or $HyPer_{cytosol}$; Evrogen) or 5 pmol of dsRNA (ALDH2, Rn01_00096063; Sigma) were diluted in 50 μl of Opti-MEM reagent (Invitrogen) and later combined with Lipofectamine (2 μl). Lipoplexes were directly added to the cells in antibiotic- and serum-free culture medium and incubated for 60 min at 37°C and 5% CO_2. Serum and antibiotics were added to the culture medium at the end of the procedure.

Adult mouse ventricular myocytes isolation and culture

Adult mouse ventricular myocytes (AMVMs) were isolated from the hearts of adult (12 weeks) male MAO-$B^{-/-}$ mice and their WT littermates as described previously (25). Cells were plated at a nonconfluent density of 25,000 rod shaped cells/ml on glass coverslips precoated with laminin (20 μg/ml) and kept at 37°C in the culture medium (Joklik modified MEM, $NaHCO_3$ 2 g/l, BSA 5 g/l, L-carnitine 1.5 mM, creatine 5 mM, taurine 7.5 mM, ITS 1%, penicillin 100 IU/ml, streptomycin 10 μg/ml) for 1 h before being used for the experiments. For mitochondrial ROS production measurements, cells were loaded with 250 nM Mitotracker Red CM-H_2XRos for 30 min at 37°C, washed and then incubated with dopamine (1.5 μM) or vehicle for 2 h. After this incubation time, cells were analyzed and images acquired by confocal microscopy. For the studies of mitochondrial membrane potential, AMVMs were preincubated with 25 nM TMRM in the presence of 1.6 μM cyclosporin H for 40 min. For the experiments employing oligomycin, AMVMs were first shortly incubated with dopamine (10 μM, to activate MAO-B) and then 25 μM oligomycin was added and kinetics was followed by confocal microscopy. Images were analyzed and fluorescence intensities determined using computer-assisted image analysis systems (ImageJ; NIH). Approximately 100 cells were analyzed per condition in each experiment and all the experiments were repeated at least thrice.

Catecholamine measurement

Hearts were retrogradely perfused in a Langerdorff apparatus for 10 min after the excision using K-H solution to remove any contaminating blood. Then, LV specimens were dissected and homogenized in 0.4 M perchloric acid containing 0.5 mM EDTA, centrifuged at 3000 rpm for 5 min and the supernatant stored for alumina extraction. Catecholamines were determined by HPLC as described previously (18).

Western blot

Samples were prepared in SDS Laemmli buffer and DTT (65 mM). Proteins were separated using 4%–12% bis/tris polyacrylamide gel electrophoresis. Western blotting was performed using a rabbit anti-ERK1/2 and anti-pERK1/2 polyclonal antibody (1:1000 dilution; Cell Signaling) and an IRDye 800CW–labeled donkey anti-rabbit antibody (1:10,000 dilution; LI-COR Biosciences). ALDH2 was visualized using a primary mouse monoclonal antibody (1:1000 dilution, WH0000217M1; Sigma) and an anti-mouse secondary (1:2000; Pierce). Densitometry analysis was performed using LI-COR Odyssey software.

Statistics

All values are expressed as mean ± SEM. Comparison between groups was performed by one-way or two-way ANOVA, followed by a Tukey's *post hoc* multiple comparison test. Comparisons between two groups were performed using nonpaired two-tailed Student's t-test. A value of $p < 0.05$ was considered significant.

Acknowledgments

We would like to thank Raymond Johnson from the Vanderbilt Neurochemistry Core Laboratory and Dr. Randy Blakely for their help with HPLC measurements and helpful discussions. This work has been supported by MIUR, CNR and Cariparo (F.D.L.), by the Fondation Leducq (V.S. and D.A.K.), the Peter Belfer Laboratory, and the Abraham and Virginia Weiss Professorship (D.A.K.), NIH (R01MH39085 to J.C.S., R01HL075265 and R01HL091923 to N.P.).

Author Disclosure Statement

No competing financial interests exist.

References

1. Alnouti Y and Klaassen CD. Tissue distribution, ontogeny, and regulation of aldehyde dehydrogenase (Aldh) enzymes mRNA by prototypical microsomal enzyme inducers in mice. *Toxicol Sci* 101: 51–64, 2008.
2. Aries A, Paradis P, Lefebvre C, Schwartz RJ, and Nemer M. Essential role of GATA-4 in cell survival and drug-induced cardiotoxicity. *Proc Natl Acad Sci U S A* 101: 6975–6980, 2004.

3. Backs J, Haunstetter A, Gerber SH, Metz J, Borst MM, Strasser RH, Kubler W, and Haass M. The neuronal norepinephrine transporter in experimental heart failure: evidence for a posttranscriptional downregulation. *J Mol Cell Cardiol* 33: 461–472, 2001.
4. Beau SL and Saffitz JE. Transmural heterogeneity of norepinephrine uptake in failing human hearts. *J Am Coll Cardiol* 23: 579–585, 1994.
5. Bianchi P, Kunduzova O, Masini E, Cambon C, Bani D, Raimondi L, Seguelas MH, Nistri S, Colucci W, Leducq N, and Parini A. Oxidative stress by monoamine oxidase mediates receptor-independent cardiomyocyte apoptosis by serotonin and postischemic myocardial injury. *Circulation* 112: 3297–3305, 2005.
6. Bianchi P, Pimentel DR, Murphy MP, Colucci WS, and Parini A. A new hypertrophic mechanism of serotonin in cardiac myocytes: receptor-independent ROS generation. *FASEB J* 19: 641–643, 2005.
7. Bortolato M, Chen K, and Shih JC. Monoamine oxidase inactivation: from pathophysiology to therapeutics. *Adv Drug Deliv Rev* 60: 1527–1533, 2008.
8. Bueno OF, De Windt LJ, Tymitz KM, Witt SA, Kimball TR, Klevitsky R, Hewett TE, Jones SP, Lefer DJ, Peng CF, Kitsis RN, and Molkentin JD. The MEK1-ERK1/2 signaling pathway promotes compensated cardiac hypertrophy in transgenic mice. *EMBO J* 19: 6341–6350, 2000.
9. Burke WJ, Li SW, Chung HD, Ruggiero DA, Kristal BS, Johnson EM, Lampe P, Kumar VB, Franko M, Williams EA, and Zahm DS. Neurotoxicity of MAO metabolites of catecholamine neurotransmitters: role in neurodegenerative diseases. *Neurotoxicology* 25: 101–115, 2004.
10. Carpi A, Menabo R, Kaludercic N, Pelicci P, Di Lisa F, and Giorgio M. The cardioprotective effects elicited by p66(Shc) ablation demonstrate the crucial role of mitochondrial ROS formation in ischemia/reperfusion injury. *Biochim Biophys Acta* 1787: 774–780, 2009.
11. Chen CH, Budas GR, Churchill EN, Disatnik MH, Hurley TD, and Mochly-Rosen D. Activation of aldehyde dehydrogenase-2 reduces ischemic damage to the heart. *Science* 321: 1493–1495, 2008.
12. Chen CH, Sun L, and Mochly-Rosen D. Mitochondrial aldehyde dehydrogenase and cardiac diseases. *Cardiovasc Res* 88: 51–57, 2010.
13. Cingolani OH and Kass DA. Pressure-volume relation analysis of mouse ventricular function. *Am J Physiol Heart Circ Physiol* 301: H2198–H2206, 2011.
14. Diwan A and Dorn GW. Decompensation of cardiac hypertrophy: cellular mechanisms and novel therapeutic targets. *Physiology (Bethesda)* 22: 56–64, 2007.
15. Dorris RL. A simple method for screening monoamine oxidase (MAO) inhibitory drugs for type preference. *J Pharmacol Methods* 7: 133–137, 1982.
16. Eisenhofer G. The role of neuronal and extraneuronal plasma membrane transporters in the inactivation of peripheral catecholamines. *Pharmacol Ther* 91: 35–62, 2001.
17. Eisenhofer G, Friberg P, Rundqvist B, Quyyumi AA, Lambert G, Kaye DM, Kopin IJ, Goldstein DS, and Esler MD. Cardiac sympathetic nerve function in congestive heart failure. *Circulation* 93: 1667–1676, 1996.
18. Eisenhofer G, Goldstein DS, Stull R, Keiser HR, Sunderland T, Murphy DL, and Kopin IJ. Simultaneous liquid-chromatographic determination of 3,4-dihydroxyphenylglycol, catecholamines, and 3,4-dihydroxyphenylalanine in plasma, and their responses to inhibition of monoamine oxidase. *Clin Chem* 32: 2030–2033, 1986.
19. Georgakopoulos D and Kass DA. Protocols for hemodynamic assessment of transgenic mice *in vivo*. *Methods Mol Biol* 219: 233–243, 2003.
20. Grimsby J, Toth M, Chen K, Kumazawa T, Klaidman L, Adams JD, Karoum F, Gal J, and Shih JC. Increased stress response and beta-phenylethylamine in MAOB-deficient mice. *Nat Genet* 17: 206–210, 1997.
21. Hauptmann N, Grimsby J, Shih JC, and Cadenas E. The metabolism of tyramine by monoamine oxidase A/B causes oxidative damage to mitochondrial DNA. *Arch Biochem Biophys* 335: 295–304, 1996.
22. Himura Y, Felten SY, Kashiki M, Lewandowski TJ, Delehanty JM, and Liang CS. Cardiac noradrenergic nerve terminal abnormalities in dogs with experimental congestive heart failure. *Circulation* 88: 1299–1309, 1993.
23. Irwin WA, Bergamin N, Sabatelli P, Reggiani C, Megighian A, Merlini L, Braghetta P, Columbaro M, Volpin D, Bressan GM, Bernardi P, and Bonaldo P. Mitochondrial dysfunction and apoptosis in myopathic mice with collagen VI deficiency. *Nat Genet* 35: 367–371, 2003.
24. Kaludercic N, Carpi A, Menabo R, Di Lisa F, and Paolocci N. Monoamine oxidases (MAO) in the pathogenesis of heart failure and ischemia/reperfusion injury. *Biochim Biophys Acta* 1813: 1323, 2011.
25. Kaludercic N, Takimoto E, Nagayama T, Feng N, Lai EW, Bedja D, Chen K, Gabrielson KL, Blakely RD, Shih JC, Pacak K, Kass DA, Di Lisa F, and Paolocci N. Monoamine oxidase A-mediated enhanced catabolism of norepinephrine contributes to adverse remodeling and pump failure in hearts with pressure overload. *Circ Res* 106: 193–202, 2010.
26. Kehat I and Molkentin JD. Extracellular signal-regulated kinase 1/2 (ERK1/2) signaling in cardiac hypertrophy. *Ann N Y Acad Sci* 1188: 96–102, 2010.
27. Lairez O, Calise D, Bianchi P, Ordener C, Spreux-Varoquaux O, Guilbeau-Frugier C, Escourrou G, Seif I, Roncalli J, Pizzinat N, Galinier M, Parini A, and Mialet-Perez J. Genetic deletion of MAO-A promotes serotonin-dependent ventricular hypertrophy by pressure overload. *J Mol Cell Cardiol* 46: 587–595, 2009.
28. Liang CS, Fan TH, Sullebarger JT, and Sakamoto S. Decreased adrenergic neuronal uptake activity in experimental right heart failure. A chamber-specific contributor to beta-adrenoceptor downregulation. *J Clin Invest* 84: 1267–1275, 1989.
29. Maser RE and Lenhard MJ. Cardiovascular autonomic neuropathy due to diabetes mellitus: clinical manifestations, consequences, and treatment. *J Clin Endocrinol Metab* 90: 5896–5903, 2005.
30. Nozawa T, Igawa A, Yoshida N, Maeda M, Inoue M, Yamamura Y, Asanoi H, and Inoue H. Dual-tracer assessment of coupling between cardiac sympathetic neuronal function and downregulation of beta-receptors during development of hypertensive heart failure of rats. *Circulation* 97: 2359–2367, 1998.
31. Pchejetski D, Kunduzova O, Dayon A, Calise D, Seguelas MH, Leducq N, Seif I, Parini A, and Cuvillier O. Oxidative stress-dependent sphingosine kinase-1 inhibition mediates monoamine oxidase A-associated cardiac cell apoptosis. *Circ Res* 100: 41–49, 2007.
32. Pop-Busui R, Kirkwood I, Schmid H, Marinescu V, Schroeder J, Larkin D, Yamada E, Raffel DM, and Stevens MJ. Sympathetic dysfunction in type 1 diabetes: association with

impaired myocardial blood flow reserve and diastolic dysfunction. *J Am Coll Cardiol* 44: 2368–2374, 2004.
33. Purcell NH, Wilkins BJ, York A, Saba-El-Leil MK, Meloche S, Robbins J, and Molkentin JD. Genetic inhibition of cardiac ERK1/2 promotes stress-induced apoptosis and heart failure but has no effect on hypertrophy *in vivo*. *Proc Natl Acad Sci U S A* 104: 14074–14079, 2007.
34. Rees JN, Florang VR, Eckert LL, and Doorn JA. Protein reactivity of 3,4-dihydroxyphenylacetaldehyde, a toxic dopamine metabolite, is dependent on both the aldehyde and the catechol. *Chem Res Toxicol* 22: 1256–1263, 2009.
35. This reference has been deleted.
36. Sivasubramaniam SD, Finch CC, Rodriguez MJ, Mahy N, and Billett EE. A comparative study of the expression of monoamine oxidase-A and -B mRNA and protein in non-CNS human tissues. *Cell Tissue Res* 313: 291–300, 2003.
37. Takimoto E, Champion HC, Li M, Belardi D, Ren S, Rodriguez ER, Bedja D, Gabrielson KL, Wang Y, and Kass DA. Chronic inhibition of cyclic GMP phosphodiesterase 5A prevents and reverses cardiac hypertrophy. *Nat Med* 11: 214–222, 2005.
38. Takimoto E, Champion HC, Li M, Ren S, Rodriguez ER, Tavazzi B, Lazzarino G, Paolocci N, Gabrielson KL, Wang Y, and Kass DA. Oxidant stress from nitric oxide synthase-3 uncoupling stimulates cardiac pathologic remodeling from chronic pressure load. *J Clin Invest* 115: 1221–1231, 2005.
39. Takimoto E and Kass DA. Role of oxidative stress in cardiac hypertrophy and remodeling. *Hypertension* 49: 241–248, 2007.
40. Takimoto E, Yao A, Toko H, Takano H, Shimoyama M, Sonoda M, Wakimoto K, Takahashi T, Akazawa H, Mizukami M, Nagai T, Nagai R, and Komuro I. Sodium calcium exchanger plays a key role in alteration of cardiac function in response to pressure overload. *FASEB J* 16: 373–378, 2002.
41. Teiger E, Than VD, Richard L, Wisnewsky C, Tea BS, Gaboury L, Tremblay J, Schwartz K, and Hamet P. Apoptosis in pressure overload-induced heart hypertrophy in the rat. *J Clin Invest* 97: 2891–2897, 1996.
42. Villeneuve C, Guilbeau-Frugier C, Sicard P, Lairez O, Ordener C, Duparc T, De PD, Couderc B, Spreux-Varoquaux O, Tortosa F, Garnier A, Knauf C, Valet P, Borchi E, Nediani C, Gharib A, Ovize M, Delisle MB, Parini A, and Mialet-Perez J. p53-PGC-1alpha pathway mediates oxidative mitochondrial damage and cardiomyocyte necrosis induced by monoamine oxidase-a upregulation: role in chronic left ventricular dysfunction in mice. *Antioxid Redox Signal* 18: 5–18, 2013.
43. Youdim MB, Edmondson D, and Tipton KF. The therapeutic potential of monoamine oxidase inhibitors. *Nat Rev Neurosci* 7: 295–309, 2006.
44. Zhang Y, Babcock SA, Hu N, Maris JR, Wang H, and Ren J. Mitochondrial aldehyde dehydrogenase (ALDH2) protects against streptozotocin-induced diabetic cardiomyopathy: role of GSK3beta and mitochondrial function. *BMC Med* 10: 40, 2012.

Address correspondence to:
Dr. Nazareno Paolocci
Division of Cardiology
Johns Hopkins Medical Institutions
Ross 858
720 Rutland Ave.
Baltimore, MD 21205

E-mail: npaoloc1@jhmi.edu

Date of first submission to ARS Central, March 22, 2012; date of final revised submission, April 4, 2013; date of acceptance, April 14, 2013.

Abbreviations Used

4-HNE = 4-hydroxynonenal
ALDH = aldehyde dehydrogenase
BW = body weight
DOPAC = 3,4-dehydroxyphenylacetic acid
DOPAL = 3,4-dehydroxyphenylacetaldehyde
EDV = end-diastolic volume
EF = ejection fraction
ERK = extracellular signal regulated kinase
ESV = end-systolic volume
FCCP = carbonyl cyanide 4-(trifluoromethoxy) phenylhydrazone
FS = fractional shortening
I/R = ischemia/reperfusion
IVS = interventricular septum
LV = left ventricular
LVEDD = left ventricular end-diastolic dimension
LVESD = left ventricular end-systolic dimension
LVPW = left ventricular posterior wall
MAO = monoamine oxidase
PRSW = preload-recruitable stroke work
PV = pressure-volume
ROS = reactive oxygen species
TAC = transverse aortic constriction
TMRM = tetramethylrhodamine methyl ester
TUNEL = terminal deoxynucleotidyl transferase dUTP nick end labeling
WT = wild type